

Short- and long-range order of the binary Madelung lattice

C. Wolverton and Alex Zunger

National Renewable Energy Laboratory, Golden, Colorado 80401

(Received 14 November 1994)

We discuss the influence of point-ion electrostatics on the long- (LRO) and short-range order (SRO) in binary fcc-, bcc-, and simple-cubic- (sc) based alloys. The electrostatic problem is studied by a combination of (a) a model for the distribution of point charges on lattice sites, motivated by recent first-principles calculations, (b) a mapping of the infinite-ranged Coulomb interaction onto a rapidly convergent series of effective interactions, and (c) Monte Carlo simulated annealing of the ensuing Ising-like expansion. This provides a means to identify the lowest energy structures ("ground states") at zero temperature and the dominant wave vectors of the SRO at high temperatures, which are stabilized by ionic interactions. (i) We confirm previous results that the three ground states of the fcc Madelung lattice are the $D0_{22}$ (A_3B and AB_3) and "40" (AB) structures, which can all be described as $\langle 210 \rangle$ superlattices. We further find that the ground states of the bcc and sc Madelung lattices are CsCl and NaCl, respectively. (ii) Despite the fact that the structure "40" has the lowest electrostatic energy of any fcc-type compound, this structure is very rare in nature. We find that this rarity could imply that a *highly ionic* fcc AB compound will transform to the bcc structure CsCl that is electrostatically more stable for the same charge distribution. The exception is when the energy required to promote the *elemental solids* $A + B$ from fcc to bcc is larger than the gain in electrostatic energy. (iii) Monte Carlo and mean-field calculations both demonstrate that the dominant wave vectors of LRO and SRO coincide for the bcc and sc Madelung lattices. However, for compositions $x \lesssim 0.33$ and $x \gtrsim 0.67$ on the fcc lattice, mean-field calculations incorrectly predict SRO peaks at the $\langle 1\frac{1}{2}0 \rangle$ points, whereas Monte Carlo calculations show SRO peaks at the $\langle 100 \rangle$ points. Thus, in describing fcc electrostatics, the mean-field theory of SRO is seen to qualitatively fail. (iv) Electrostatic point-ion interactions lead to significant SRO correlations. Near the transition temperature, these correlations account for a $\gtrsim 60\%$ change in the energy of the random alloy.

I. INTRODUCTION: THE MADELUNG LATTICE PROBLEM

When different atoms are brought together to form an alloy or compound, the redistribution of charge densities as compared to their atomic densities may lead to what is commonly referred to as "charge transfer." The electrostatic contributions to the total energy of an alloy or compound due to charge transfer have been widely used to discuss the structural stability of not only alkali halides,¹ but also coordination compounds^{2,3} and semiconductor⁴ and intermetallic alloys.⁵⁻⁸ Whereas in *ab initio* total energy calculations^{9,10} the electrostatic contribution is calculated from the *continuous* electronic charge density $\rho(\mathbf{r})$, in simpler approaches one discretizes the (electronic plus nuclear) charge density into a set of *point* charges. The ensuing electrostatic Madelung (M) energy E_M has been widely used as one of the energy terms deciding structural stability of compounds and alloys.^{1-3,5-7} We discuss in this paper the manner in which the point-ion electrostatics decides the long- and short-range order in binary fcc-, bcc-, and simple-cubic- (sc) based alloys. While the electrostatic contribution is clearly not the only term entering the total energy, it is interesting to see that it leads to clear structural preferences for both short- and long-range order.

In the point-ion Madelung model^{11,12} of a given lattice (e.g., fcc, bcc, and sc), each of the $N \rightarrow \infty$ sites

$i = 1, 2, \dots, N$ is assigned a net charge Q_i and is occupied by either an A atom (denoted by a spin variable $\hat{S}_i = -1$) or a B atom (denoted by $\hat{S}_i = +1$). The Madelung energy $E_M(\sigma)$ of each of the possible 2^N alloy configurations σ can be written as an infinite-range Ising-type Hamiltonian

$$E_M(\sigma) = \frac{1}{2N} \sum'_{i,j} \frac{Q_i Q_j}{|\mathbf{d}_i - \mathbf{d}_j|} = \frac{1}{2N} \sum'_{i,j} \hat{S}_i \hat{S}_j J_{ij}(\sigma), \quad (1)$$

where the primed sum is over all pairs of lattice sites i and j , excluding the $i = j$ terms, and $|\mathbf{d}_i - \mathbf{d}_j|$ represents the distance between lattice sites i and j . The bare, pairwise Coulomb interaction energy J_{ij} can be written as

$$J_{ij}(\sigma) = \frac{Q_i Q_j}{|\mathbf{d}_i - \mathbf{d}_j|} \hat{S}_i \hat{S}_j. \quad (2)$$

While nonelectrostatic bonding effects can certainly stabilize a given crystal structure, it is interesting to determine which structures σ have the lowest *electrostatic* energy for a given type of lattice (e.g., fcc, bcc, and sc). Although it is possible to use standard Ewald techniques¹² to evaluate $E_M(\sigma)$ for some simple configurations σ (e.g., simple ordered $A_n B_m$ structures), extension of this "direct" approach to the 2^N configurations appearing in an $A_{1-x} B_x$ alloy is complicated by two factors.

First, evaluating $E_M(\sigma)$ from Ewald's method for *all* possible 2^N configurations of N lattice sites occupied by A and B atoms can be laborious. This problem can be addressed by using lattice-gas techniques which efficiently search the 2^N space for the lowest energy configurations.^{13,14} However, in the formulation of Eqs. (1) and (2), the bare interactions J_{ij} are infinite in range and are dependent upon the configuration through the configuration dependence of the charges Q_i . Both these facts make the Ising series written in terms of the *bare* interactions cumbersome, as much of the literature to date on Ising models¹⁵⁻¹⁷ concerns interactions which are relatively short ranged and configuration independent. However, as shown recently,¹⁸ it is possible to *exactly* renormalize the infinite ranged series of Eq. (1) expressed in terms of *bare* Coulomb interactions into a short-ranged, highly convergent series expressed in terms of *effective* interactions which are configuration independent. This will be illustrated in Sec. II. Hence the standard techniques used to deal with Ising models¹⁵⁻¹⁷ may be applied to this series of effective interactions.

The second difficulty with a direct search of $E_M(\sigma)$ is that this requires a model associating sites i with charges Q_i . The association of sites and charges is not trivial except for the cases of ordered arrangements of atoms for which all chemically identical atoms are also symmetry equivalent and hence have identical local environments. For instance, in the perfectly ordered NaCl structure, all Na sites i have only Cl atoms as nearest neighbors and thus can be assigned the charges $Q_i = +1$ for all i . Similarly, all Cl sites j are surrounded exclusively by Na and have $Q_j = -1$ for all j . However, in a random $\text{Na}_{0.5}\text{Cl}_{0.5}$ alloy, some Na atoms are coordinated locally only by Na atoms and hence have $Q_i \sim 0$, like in metallic Na, while other Na atoms could be surrounded locally by all Cl atoms and consequently could have $Q_i \sim +1$, like in the ionic NaCl crystal. Thus, in order to use Eq. (1) to realistically model the electrostatics in alloys, one must first determine a physically reasonable description for the distribution of charges on lattice sites. Recent first-principles charge density calculations for both ordered and disordered transition metal^{20,21} and semiconductor²² alloys have shown that the effective charge on each site primarily depends on the identity of atoms in the *nearest-neighbor coordination shell around it*, e.g., the number of *unlike* nearest neighbors. This suggests that a realistic model in screened solids²³ is one with a *linear* dependence of the charge on the number of unlike nearest neighbors:

$$Q_i = \lambda \sum_{k=1}^Z [\hat{S}_i - \hat{S}_{i+k}], \quad (3)$$

where \hat{S}_i is -1 ($+1$) if an A (B) atom is located at site i . \hat{S}_{i+k} indicates the occupation of the Z lattice sites which are nearest neighbors to i and hence the summation in Eq. (3) indicates the number of unlike nearest neighbors surrounding the site i . λ is a constant that indicates the magnitude of the charge transfer. The maximum possible amount of charge transfer $Q_{\max} = 2Z\lambda$ is then given by Eq. (3) for an atom coordinated completely by

unlike nearest neighbors. For example, in the fcc lattice the coordination number is $Z=12$, so the charge on an A atom surrounded by n B atoms and $12 - n$ A atoms is $Q_i = 2\lambda n$. As $0 \geq n \geq 12$, we have $0 \geq Q_i \geq 24\lambda$ depending on the value of n . Using the charge model of Eq. (3), *deduced* from first-principles calculations²⁰ and more recently derived from the coherent-potential approximation,²¹ the lattice Madelung energy may be written as

$$E_M(\sigma) = -\frac{Q_{\text{op}}^2}{2d} \alpha_M(\sigma), \quad (4)$$

where $\alpha_M(\sigma)$ is the Madelung constant for the configuration σ , d is the nearest-neighbor distance, and Q_{op} is the optimum amount of charge transfer possible for simple, ordered arrangements of atoms with only two symmetry-distinct types of atoms. The Madelung energy [Eq. (4)] is purely attractive and thus $E_M \rightarrow -\infty$ as $d \rightarrow 0$. Therefore, we optimize the Madelung *constant* α_M rather than the Madelung *energy* of Eq. (4). This is equivalent to finding the states of minimum Madelung energy for a fixed value of d and Q_{op} . Considering the CuAu, CsCl, and NaCl structures (based on the fcc, bcc, and sc lattices, respectively), we have $Q_{\text{op}} = 16\lambda$, 16λ , and 12λ . For the bcc and sc lattices, $Q_{\text{op}} = Q_{\max} = 16\lambda$ and 12λ , respectively, since for these lattice types it is possible to completely satisfy the ordering tendencies of alloys with structures in which each atom is coordinated locally completely by nearest-neighbor atoms of unlike type. Thus the bcc and sc lattices are said to be *unfrustrated*. However, the *frustrated* fcc lattice contains triangles of nearest-neighbor bonds and hence it is not possible to surround every atom on the fcc lattice with nearest neighbors of unlike type. Thus the optimal charge for the fcc lattice is $Q_{\text{op}} = \frac{2}{3}Q_{\max} = 16\lambda$. Throughout this paper, we use the energy units of $(16\lambda)^2/2d$ for the fcc and bcc lattices and for the sc lattice we use the energy unit $(12\lambda)^2/2d$.

Magri *et al.*¹⁹ and Lu *et al.*²⁴ (see the review in Ref. 18) have recently used the model of Eqs. (1) and (3) ("the binary Madelung alloy problem") in conjunction with a cluster expansion technique (to be described below) to determine for the fcc lattice (i) the ordered structures σ which maximize $\alpha_M(\sigma)$ ("ground state structures") and (ii) the energy of the completely random alloy. In addition to the pure constituents A and B , they identified three structures (Fig. 1) that are ground states of the fcc Madelung lattice: $D0_{22}$ (A_3B and AB_3) and "40" (AB). These compounds may all be described in terms of composition-waves along the $\langle 1\frac{1}{2}0 \rangle$ direction in reciprocal space or as superlattices with layers oriented along $\langle 210 \rangle$.¹⁵ They also found that the Madelung energy of the completely random state was nonvanishing, in contrast to previously accepted views.^{25,26} Thus previous studies^{19,24,18} of the binary fcc Madelung lattice have examined the cases of *complete order* (the zero-temperature states) and *complete disorder* (pertinent to infinite temperature), but did not consider the myriad of possible states of partial long- and short-range order which will be discussed here (for the fcc, bcc, and sc Madelung lattices).

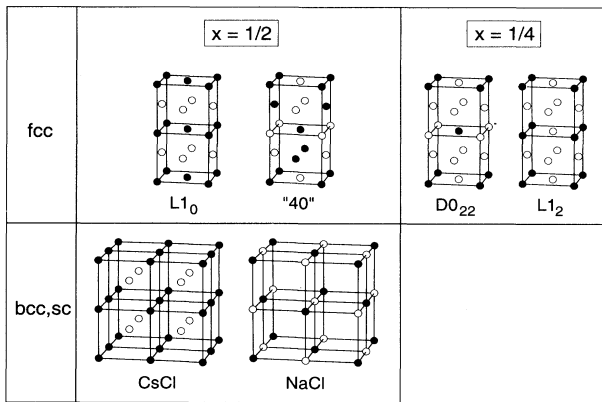


FIG. 1. Conventional unit cells for the ground state structures of the fcc, bcc, and sc Madelung lattice. In addition to the lowest energy states of each lattice, the energetically competitive $L1_0$ and $L1_2$ fcc-based structures are shown.

In this paper, we focus on several problems regarding the Madelung lattice.

(i) Although the equimolar $\langle 1\frac{1}{2}0 \rangle$ structure ("40") is a ground state of the fcc Madelung lattice,¹⁹ surprisingly it is rarely if ever observed experimentally in fcc-based alloys.²⁷ Given that Eq. (3) was demonstrated^{20,21} to be an excellent approximation to direct local-density approximation (LDA) calculations, one must conclude that either charge transfer is *never* the dominant effect at equiatomic composition or when it is dominant, geometrical factors such as lattice topology serve to make other *non-fcc* structures more stable. We find that the CsCl structure has the highest Madelung constant (and consequently, the lowest energy) of any fcc-, bcc-, or sc-based structure. Hence, even in alloy systems where charge transfer is a dominant effect, an fcc alloy would prefer to transform to the bcc CsCl structure, which, for the same ionic charges, produces the *maximal* electrostatic stabilization. An exception would occur for an ionic alloy system with fcc constituents for which the energy required to promote the elemental solids from fcc to bcc more than outweighs the gain in electrostatic energy upon going from the fcc-based "40" to the bcc-based CsCl structure. The promotion energies also provide an explanation for the absence of the NaCl structure in transition metal alloys. The NaCl structure has the lowest electrostatic energy of any sc-based compound (and is very close in Madelung energy to the CsCl structure). However, the NaCl structure is never observed in transition metal alloys because the energy required to promote the elemental metals (usually in the fcc, bcc, or hcp structures) to the sc structure is quite large and overcomes the large negative electrostatic energy of NaCl.

(ii) Given that the long-range order (LRO) of the fcc Madelung lattice is of $\langle 1\frac{1}{2}0 \rangle$ type, we will determine the dominant wave vectors of the *short-range order* (SRO). Although mean-field theories often equate the dominant wave vectors of SRO with those of LRO,²⁸ recent experiments²⁹ and calculations^{30,31} have demonstrated that the dominant wave vectors of LRO and SRO need not necessarily coincide. Therefore, it is of interest

to determine the SRO of the Madelung lattice, both by mean-field and non-mean-field (Monte Carlo) methods. We find that for the unfrustrated bcc and sc lattices, the mean-field description of SRO provides accurate results as compared with the Monte Carlo calculations for all alloy compositions x . However, for the fcc Madelung lattice at compositions $x \lesssim 0.33$ and $x \gtrsim 0.67$, the mean-field theory gives a *qualitatively incorrect* description of the SRO. The qualitative failure of the mean-field theory for $x = \frac{1}{4}$, but not $x = \frac{1}{2}$, will be explained by considering simple, model calculations that demonstrate the ranges of interactions for which the mean-field SRO may be expected to fail. The failure of the mean-field theory of SRO for the fcc Madelung lattice has important consequences in light of its nearly universal use in the field of SRO calculations based on the concentration-wave extension of the coherent-potential approximation (CPA).^{26,32-35}

(iii) Recently, a simple ("Onsager") correction has been proposed to the mean-field SRO. We find that the "Onsager-corrected" SRO fails in precisely the same manner [see (ii) above] as the uncorrected mean-field SRO.

(iv) We wish to determine whether the energy and temperature scales pertinent to the Madelung energy are relevant on the scale of typical heats of formation and the temperatures at which SRO is normally measured. We find that the scale of the Madelung contribution to the energetics of random alloys may be quite sizeable (in some cases, inclusion of Madelung energies even results in a change of sign in the heat of formation). It is also of interest to compare the magnitudes of the energetic contributions of the Madelung energies which are due to the completely random alloy with those due to short-range order. We find that the Madelung energy leads to significant SRO correlations which account for a $\gtrsim 60\%$ change in the energy of the completely random alloy. Thus any attempt to compare calculated heats of formation in disordered alloys with those of experiment should include not only the Madelung energy of the *random* alloy, but also the contribution due to SRO as well.

The remainder of the paper is organized as follows. In Sec. II we describe how the Madelung energy expressed in terms of infinite-ranged bare interactions may be exactly mapped onto a highly convergent cluster expansion in terms of effective interactions. Analytic expressions for the effective interactions are presented and evaluated. Section III contains a description of how simulated annealing may be used in conjunction with the cluster expansion to determine the ground states, transition temperatures, and short-range order of the model. The ground state results are given in Sec. IV A, and the competition between Madelung and structural promotion energies is discussed in Sec. IV B. The SRO is given for the bcc and sc Madelung lattices in Sec. IV C and for the fcc Madelung lattice in Sec. IV D. Implications of the failure of the mean-field theory of SRO are given in Sec. IV E and the magnitude of various contributions to the energy and temperature scales presented here are examined in Sec. IV F. A brief summary of the results is given in Sec. V.

II. ANALYTIC CLUSTER EXPANSION OF THE MADELUNG LATTICE

To compute the LRO and SRO for the Madelung lattice, we first show how the series of Eq. (1) in terms of infinite-range *bare* interactions (J_{ij}) may be exactly mapped onto a rapidly convergent cluster expansion (CE) in terms of *effective* interactions (\tilde{J}_f):¹⁴

$$\alpha_{\text{CE}}(\sigma) = \sum_f D_f \tilde{J}_f \bar{\Pi}_f(\sigma), \quad (5)$$

where f is a figure comprised of several lattice sites (pairs, triplets, etc.), D_f is the number of symmetry-equivalent figures per lattice site, and \tilde{J}_f is the *effective* interaction for the figure f . The function $\bar{\Pi}_f$ is defined¹⁴ as a product over the figure f of the variables S_i , with the overbar denoting an average over all symmetry equivalent figures of lattice sites.

To gain some insight into the nature of the *effective* interactions \tilde{J}_f , one may utilize the orthonormal properties of the functions $\Pi_f(\sigma)$ to obtain the following expression:

$$\begin{aligned} \tilde{J}_f &= \frac{1}{2^N} \sum_{\sigma} \alpha_M(\sigma) \Pi_f(\sigma) \\ &= \frac{-d}{2^N N Q_{\text{op}}^2} \sum_{\sigma} \Pi_f(\sigma) \sum_{i,j} ' \hat{S}_i \hat{S}_j J_{ij}(\sigma), \end{aligned} \quad (6)$$

where $\alpha_M(\sigma)$ are the *exact* Madelung constants obtained, for example, from the Ewald method. We see that the effective interaction \tilde{J}_f for any given figure f (e.g., the *first* nearest-neighbor pair) is a sum over configurations σ of Madelung constants, each representing an infinite sum over *all* pairs [Eq. (1)]. Thus, even the relatively short-ranged *effective* interactions \tilde{J}_f represent an infinite sum over all of the *bare* pair interactions J_{ij} . Note that the effective interactions \tilde{J}_f represent the expansion coefficients of the Madelung *constant* of Eq. (4) and thus have opposite signs from the expansion coefficients of the Madelung *energy*.

Due to the orthonormality and completeness of the basis functions¹⁴ Π_f , the cluster expansion of Eq. (5) is an *exact* representation of any function of alloy configuration, such as Eq. (1). Furthermore, due to the relatively simple nature of the model of charges on the sites [Eq. (3)], the effective interactions \tilde{J}_f may be derived analytically by combining Eqs. (1), (3), and (6) and¹⁸ using the orthonormal properties of Π_f . The result is

$$\tilde{J}_f / \left(\frac{-\lambda^2 d}{N Q_{\text{op}}^2} \right) = \sum_{i,j} ' \frac{1}{d_{ij}} \sum_{k,k'} [\delta_{f,ij} - \delta_{f,ik'} - \delta_{f,jk} + \delta_{f,kk'}], \quad (7)$$

and

$$\tilde{J}_0 / \left(\frac{-\lambda^2 d}{N Q_{\text{op}}^2} \right) = \sum_{i,j} ' \frac{1}{d_{ij}} \sum_{k,k'} [-\delta_{i,k'} - \delta_{j,k} + \delta_{k,k'}], \quad (8)$$

where the sums over k and k' are over all nearest neighbors of i and j , respectively, and d_{ij} represents the distance between points i and j . The Kronecker symbol $\delta_{f,ij}$ equals zero unless the figure f equals the pair figure ij (and equals one otherwise), and $\delta_{i,k'}$ equals zero unless $i = k'$ (and equals one otherwise), etc. The only nonvanishing effective interactions in Eqs. (7) and (8) are a constant interaction term (\tilde{J}_0) and those \tilde{J}_f 's corresponding to pairs of sites.

For the constant interaction term \tilde{J}_0 , the summations in Eq. (8) may be evaluated to give

$$\tilde{J}_0 / \left(\frac{\lambda^2 d}{Q_{\text{op}}^2} \right) = \frac{2Z_1^2}{d_1} - \sum_{m=1}^{\infty} \frac{Z_m K_m}{d_m}, \quad (9)$$

where Z_m is the coordination of the m th shell, d_m is the distance between i and $i + m$ ($d_1 = d$ is the nearest-neighbor distance), and K_m is the number of nearest-neighbor atoms shared by sites i and $i + m$. Z_m , d_m , and K_m are purely geometrical quantities of the lattice and may be obtained by inspection. These geometrical quantities are given for the fcc, bcc, and sc lattices in Table I as are the contributions from each shell m to the Madelung constant of the configurationally averaged random alloy on each lattice type. Note that K_m vanishes for all three lattices for $m \geq 6$ and thus the summa-

TABLE I. Geometrical factors of fcc, bcc, and sc lattices and the contributions of various coordination shells to the Madelung constant of the configurationally averaged equiatomic random alloy $\langle \alpha_M \rangle_R$. Madelung constants are given with respect to the nearest-neighbor distance d of each lattice type and the charges $Q_{\text{op}} = 16\lambda$, 16λ , and 12λ for the fcc, bcc, and sc lattices, respectively.

| Lattice | m | Z_m | d_m/d | K_m | Contribution to $\langle \alpha_M \rangle_R$ |
|---------|----------|-------|------------------------------|----------------|--|
| fcc | 1 | 12 | 1 | 4 | +1.12500 - 0.18750 |
| | 2 | 6 | $\sqrt{2}$ | 4 | -0.06629 |
| | 3 | 24 | $\sqrt{3}$ | 2 | -0.10825 |
| | 4 | 12 | 2 | 1 | -0.02344 |
| | ≥ 5 | | | 0 | 0.00000 |
| | | | | | Total +0.73952 |
| bcc | 1 | 8 | 1 | 0 | +0.50000 - 0.00000 |
| | 2 | 6 | $\frac{2}{\sqrt{3}}$ | 4 | -0.08119 |
| | 3 | 12 | $\frac{2\sqrt{2}}{\sqrt{3}}$ | 2 | -0.05741 |
| | 4 | 24 | $\frac{\sqrt{11}}{\sqrt{3}}$ | 0 | 0.00000 |
| | 5 | 8 | 2 | 1 | -0.01562 |
| | ≥ 6 | | | 0 | 0.00000 |
| | | | | Total +0.34578 | |
| sc | 1 | 6 | 1 | 0 | +0.50000 - 0.00000 |
| | 2 | 12 | $\sqrt{2}$ | 2 | -0.11785 |
| | 3 | 8 | $\sqrt{3}$ | 0 | 0.00000 |
| | 4 | 6 | 2 | 1 | -0.02083 |
| | ≥ 5 | | | 0 | 0.00000 |
| | | | | Total +0.36132 | |

tion in Eq. (9) contains only a small number of nonzero terms. Also, a nonzero value of K_1 implies that there are triangles of nearest-neighbor bonds in the lattice or that the lattice is frustrated. It is then readily apparent from Table I that the fcc lattice is frustrated ($K_1 \neq 0$), but bcc and sc are not ($K_1 = 0$). Other values of K_m simply indicate the extent to which more distant pairs in the lattice are linked by common nearest neighbors. Thus K_m gives some qualitative indication of the extent to which the lattice is “open” or “close packed.” It is apparent that the fcc lattice has many more nonzero values for K_m than do bcc and sc and hence is more close packed. Similarly, the sc lattice has very few pairs of atoms which share common nearest neighbors and thus may be described as an open lattice structure. By using Eq. (9) and the geometrical quantities of Table I, the Madelung constant of the completely random (R) alloy $\langle \alpha_M \rangle_R = 4x(1-x)\tilde{J}_0$ may be evaluated analytically as a function of alloy composition:

$$\begin{aligned} \langle \alpha_M \rangle_R^{\text{fcc}} &= 4x(1-x) \left[\frac{117}{128} - \frac{3}{64}\sqrt{2} - \frac{\sqrt{3}}{16} \right] \\ &= 4x(1-x)0.7395181\dots, \end{aligned} \quad (10)$$

$$\begin{aligned} \langle \alpha_M \rangle_R^{\text{bcc}} &= 4x(1-x) \left[\frac{31}{64} - \frac{3}{128}\sqrt{6} - \frac{3}{64}\sqrt{3} \right] \\ &= 4x(1-x)0.3457752\dots, \end{aligned} \quad (11)$$

$$\begin{aligned} \langle \alpha_M \rangle_R^{\text{sc}} &= 4x(1-x) \left[\frac{23}{48} - \frac{\sqrt{2}}{12} \right] \\ &= 4x(1-x)0.3613155\dots \end{aligned} \quad (12)$$

We have evaluated the analytic expressions for not only the constant term of the cluster expansion [\tilde{J}_0 , given by Eqs. (10)–(12) evaluated at $x = 1/2$], but also the effective pair interactions [Eq. (7)] corresponding to the first 20 neighbor shells (denoted by \tilde{J}_n for the n th neighbor shell). The effective interactions are given in Table II. The extremely rapid decay of the effective pair interactions with increasing shell number n is apparent and is shown schematically in Fig. 2. This rapid convergence of the *effective* interactions is in direct contrast to the $1/d_{ij}$ decay of the *bare* interactions of Eq. (1) and is due to the effective charge screening given by the charge model of Eq. (3). For all three lattice types, the nearest-neighbor pair interaction \tilde{J}_1 is large and negative, indicative of a strong *ordering* tendency between unlike atoms or unlike charges. Beyond the fifth neighbor shell, the effective pair interactions have decayed practically to zero for all three lattices. Even within the fifth neighbor shell, the interactions often show a significant reduction in magnitude for pairs of atoms which do not share any common nearest neighbors (e.g., \tilde{J}_5 for fcc, \tilde{J}_4 for bcc, and \tilde{J}_3 and \tilde{J}_5 for sc; the nearest-neighbor interactions \tilde{J}_1 for bcc and sc are exceptions to this “rule”). It is interesting, however, that these effective pair interactions, although

TABLE II. Effective interactions \tilde{J}_f for the fcc, bcc, and sc Madelung lattices, as evaluated from the analytic expressions Eqs. (7) and (8). Given are the constant interaction term \tilde{J}_0 and the first 20 effective pair interactions \tilde{J}_{1-20} . Interactions are given with respect to the nearest-neighbor distance d of each lattice type and the charges $Q_{\text{op}} = 16\lambda$, 16λ , and 12λ for the fcc, bcc, and sc lattices, respectively. Note the rapid decay of the interactions with increasing pair separation.

| Interaction | Lattice | | |
|------------------|-------------|-------------|-------------|
| | fcc | bcc | sc |
| \tilde{J}_0 | 0.73951806 | 0.34577520 | 0.36131554 |
| \tilde{J}_1 | -0.32386629 | -0.23474035 | -0.29691074 |
| \tilde{J}_2 | 0.08253284 | 0.04413108 | 0.06108243 |
| \tilde{J}_3 | 0.06083717 | 0.04758274 | -0.00137607 |
| \tilde{J}_4 | 0.03448110 | 0.00485413 | 0.04651912 |
| \tilde{J}_5 | 0.00145513 | 0.02999447 | 0.00208957 |
| \tilde{J}_6 | 0.00047521 | -0.00155476 | 0.00072596 |
| \tilde{J}_7 | 0.00003596 | 0.00002684 | -0.00054004 |
| \tilde{J}_8 | -0.00027591 | -0.00006712 | -0.00084100 |
| \tilde{J}_9 | -0.00017215 | 0.00031621 | -0.00012596 |
| \tilde{J}_{10} | 0.00000107 | -0.00000772 | 0.00008533 |
| \tilde{J}_{11} | 0.00007166 | -0.00029827 | 0.00013433 |
| \tilde{J}_{12} | 0.00000900 | -0.00008697 | -0.00002687 |
| \tilde{J}_{13} | -0.00000998 | 0.00001475 | -0.00001079 |
| \tilde{J}_{14} | -0.00000233 | -0.00000679 | 0.00000568 |
| \tilde{J}_{15} | -0.00000771 | -0.00005639 | -0.00005213 |
| \tilde{J}_{16} | 0.00000421 | -0.00000160 | -0.00000048 |
| \tilde{J}_{17} | -0.00000613 | 0.00000659 | -0.00000604 |
| \tilde{J}_{18} | 0.00000042 | 0.00001860 | -0.00001494 |
| \tilde{J}_{19} | 0.00000225 | -0.00001356 | 0.00000871 |
| \tilde{J}_{20} | -0.00000052 | -0.00000652 | -0.00000745 |

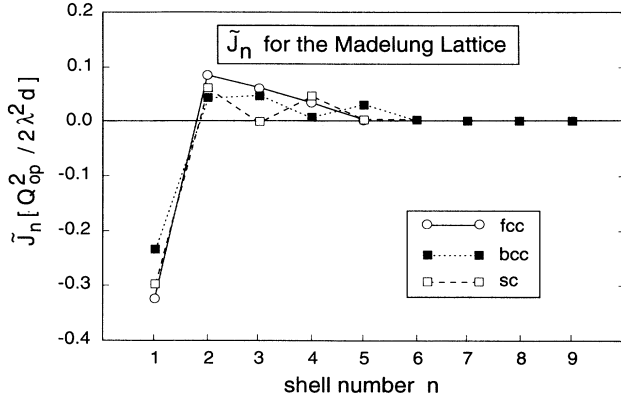


FIG. 2. Effective pair interactions for the fcc, bcc, and sc Madelung lattices. Effective pair interactions \tilde{J}_n are shown as a function of the n th-neighbor shell in units of $Q_{op}^2/2d$.

significantly reduced in magnitude, are not strictly zero. Because pairs beyond the fifth neighbor shell have extremely small effective interactions for all three lattice types, we have truncated the expansion of Eq. (5), including only \tilde{J}_n for $0 \leq n \leq 5$ for the calculations of LRO and SRO to be described below.

III. APPLICATION OF SIMULATED ANNEALING TO THE ANALYTIC CLUSTER EXPANSION

Having obtained the effective interaction energies (in units of $\lambda^2 d/Q_{op}^2$), we can now use Eq. (5) in conjunction with a Monte Carlo simulated annealing algorithm to calculate³⁶ (i) the $T=0$ K *ground state structures*, (ii) the order-disorder *transition temperatures* T_c , and (iii) the *short-range order* of the disordered solid solutions.

We use a system size of $16^3 = 4096$ atoms with periodic boundary conditions for all computations. Monte Carlo simulations were performed in the canonical ensemble for a variety of alloy concentrations $x = \frac{1}{5}, \frac{1}{4}, \frac{1}{3}$, and $\frac{1}{2}$. Due to the fact that only even-body \tilde{J}_f terms are nonzero in the cluster expansion of Eq. (1), this model is completely invariant under the transformation $x \leftrightarrow (1-x)$ ($A \leftrightarrow B$). Thus we only consider $x \leq \frac{1}{2}$, with no loss of generality. Our method of calculation is as follows.

(i) $T=0$ K ground states. The ground states are determined from the simulation at a temperature where all configurational changes proved to be energetically unfavorable. In this way, we are able to search an *extremely large* number of configurations for the lowest energy states, in contrast to many “standard” searches which consider only $O(10)$ competing structures: Approximately 10^8 changes in the atomic arrangements (“spin flips”) are performed in the simulated annealing determination of the ground states. In addition, because the Monte Carlo is based on a Metropolis algorithm, only relatively low energy states are considered, which is inherently more efficient than simply searching the configuration space at random. To verify that the simulated

annealing determination corresponds to the true ground state structure rather than a low energy metastable structure, we have also determined (for fcc \tilde{J}_{0-4} and bcc \tilde{J}_{0-5}) the Madelung lattice ground states via an *exact* linear programming solution.^{13,37} The linear programming solution of the ground state problem is exact; thus the *entire* space of 2^N configurations is included in these searches. In all cases, the ground states obtained from linear programming and simulated annealing are identical.

(ii) Order-disorder transition temperatures. Values of T_c are calculated (for first-order transitions) from the discontinuity in the internal energy as a function of temperature.

(iii) Short-range order. The Warren-Cowley SRO parameter for the n th atomic shell is related to the functions $\bar{\Pi}_f$ by

$$\text{SRO}(n) = \frac{\bar{\Pi}_{0,n} - q^2}{1 - q^2}, \quad (13)$$

where $q = 2x - 1$. We have calculated both $\text{SRO}(n)$ and its lattice Fourier transform $\text{SRO}(\mathbf{k})$ using Eq. (13) from a Monte Carlo simulated annealing prescription. The SRO is calculated using 500 Monte Carlo steps to equilibrate the system and subsequently averages are typically taken over 500 Monte Carlo steps or until a suitable convergence is achieved. Thirty-five atomic shells of $\text{SRO}(n)$ are used in all calculations, except for Fig. 8, where twenty shells are used. Our direct Monte Carlo calculations will be compared with the simple mean-field, Krivoglaz-Clapp-Moss formula²⁸

$$\text{SRO}(\mathbf{k}) = \frac{1}{1 + 4c(1-c)\tilde{J}(\mathbf{k})/kT}, \quad (14)$$

where $\tilde{J}(\mathbf{k})$ is the lattice Fourier transform of the real space \tilde{J}_f 's given above.³⁸ In the case of the fcc Madelung lattice, where there are significant discrepancies (see below) between SRO calculated via Monte Carlo [Eq. (13)] and mean-field [Eq. (14)], we also perform calculations with the mean field formula, supplemented by an “Onsager correction” Λ , as recently utilized by Staunton *et al.*:³²

$$\text{SRO}(\mathbf{k}) = \frac{1}{1 + 4c(1-c)[\tilde{J}(\mathbf{k}) - \Lambda]/kT}, \quad (15)$$

where

$$\Lambda = \int d^3\mathbf{k} \tilde{J}(\mathbf{k}) \text{SRO}(\mathbf{k}). \quad (16)$$

Equations (15) and (16) are solved self-consistently for Λ using a standard root-finding algorithm, and this value of Λ is subsequently used in Eq. (15) to determine $\text{SRO}(\mathbf{k})$. Thus we have three levels of approximation for calculating SRO: Monte Carlo [Eq. (13)], mean field [Eq. (14)], and mean field with Onsager corrections [Eqs. (15) and (16)].

IV. RESULTS

A. $T = 0$ K long-range order (“ground states”)

The LRO ground states and random energies for the fcc, bcc, and sc Madelung lattices are shown in Fig. 3. From the ground state searches, we find the following features.

(i) As in the work of Magri *et al.*, we find (in addition to the pure constituents A and B) the three lowest energy fcc-based configurations to be the $D0_{22}$ (A_3B and AB_3) and “40” (AB) structures, all of which are composed out of composition waves along the $\langle 1\frac{1}{2}0 \rangle$ direction in reciprocal space. (The $D0_{22}$ structure is composed out of a combination of $\langle 1\frac{1}{2}0 \rangle$, $\langle 100 \rangle$, and $\langle 000 \rangle$ composition waves; however, the $\langle 1\frac{1}{2}0 \rangle$ wave has the largest amplitude.) The $\langle 100 \rangle$ -based structures $L1_0$ (AB) and $L1_2$ (A_3B and AB_3) are, however, energetically in close competition. Conventional unit cells for all of these structures are shown in Fig. 1.

(ii) For each of the bcc and sc lattices, only *one* intermediate compound appears in the ground state analysis at equiatomic composition. These are the CsCl bcc-based and NaCl sc-based structures, which may be described by $\langle 100 \rangle$ and $\frac{1}{2}\langle 111 \rangle$ composition waves, respectively. Thus, at equiatomic composition, there is an interesting competition between the $\langle 1\frac{1}{2}0 \rangle$ -, $\langle 100 \rangle$ -, and $\frac{1}{2}\langle 111 \rangle$ -type waves for the fcc, bcc, and sc lattices. This competi-

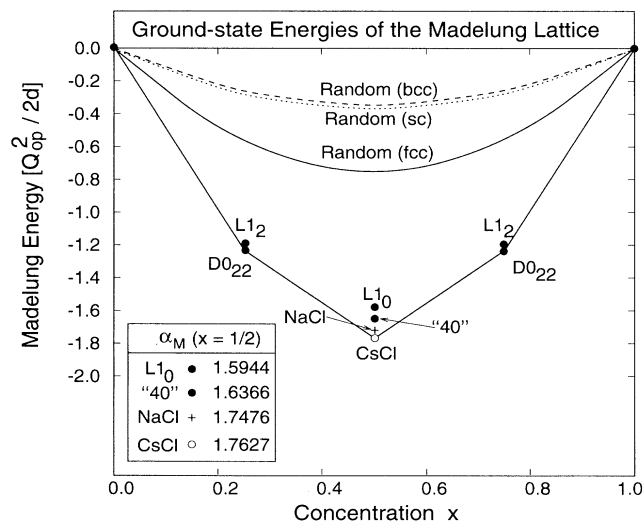


FIG. 3. Ground state structures and random energies of the fcc, bcc, and sc Madelung lattices. The fcc-, bcc-, and sc-based structures are shown as filled circles, empty circles, and crosses. In addition to the lowest energy structures on each lattice, several structures are also shown which have energies close to the ground state line. The inset shows the equiatomic structures and also gives the numerical values of the Madelung constants, as calculated from a cluster expansion with the first 20 pair interactions \tilde{J}_{0-20} (see Table II). The cluster expansion values for the Madelung constants all agree with the exact (as per the Ewald method) values to five significant digits.

tion is illustrated in greater detail in the inset of Fig. 3. Of the *ordered* equiatomic compounds, both the bcc-based CsCl and sc-based NaCl have a higher Madelung constant (lower electrostatic energy) than the fcc-based structures. The CsCl has the lowest Madelung energy (highest Madelung constant). The relative orders of electrostatic stability of the four equiatomic compounds (CsCl, NaCl, $L1_0$, and “40”) are not directly amenable to a simple nearest-neighbor-only description: If the cluster expansion of Eq. (5) is prematurely *truncated* at the first-, second-, third-, or fourth-neighbor effective interactions (Table II), the lowest energy structure at $x = 1/2$ is incorrectly predicted to be $L1_0$ (degenerate with “40”), $L1_0$, “40”, or NaCl, respectively. Only when the first five shells of effective interactions are retained (Table II) does the cluster expansion give the correct order of stability (as confirmed by Ewald-method calculations) as shown in Fig. 3. Subsequently adding more shells of effective interactions (from the 6th to the 20th neighbor shell) does not change the qualitative order of stability between the $x = 1/2$ structures and also makes a negligible quantitative change to the Madelung constants of these structures. These facts again imply the convergence of the cluster expansion of the Madelung lattice with only the first five shells of *effective* interactions.

(iii) Although the *ordered* bcc (CsCl) and sc (NaCl) structures are electrostatically more stable than those of fcc, the *random* fcc solid solutions are much lower in energy than the bcc or sc solid solutions (Fig. 3). Indeed, it is observed³⁹ in the ionic Cu-Pd system that, although the LRO at equiatomic composition is the bcc-based CsCl structure, the alloy disorders into an *fcc* solid solution. The relative energies of random alloys on different lattices are described in Eq. (9) by the subtle geometrical interplay between the effects of coordination numbers (Z_m) and the frustration of the lattice for all shells (K_m) as shown in Table I: The contributions of the first-neighbor shell to the random alloy Madelung constants already gives the fcc random alloy a Madelung constant larger than bcc or sc. However, to obtain the correct order of electrostatic stability between the bcc and sc random alloys, one must at least include up to the third-neighbor shell. Inclusion of the first- through fifth-neighbor shells gives the quantitatively *exact* result, as all terms in Eq. (9) are precisely zero for $m \geq 6$ in all three lattice types.

(iv) In Fig. 3 we have drawn the convex hull which connects the lowest energy configurations of all three lattice types. Three compounds are the ground states of the binary Madelung lattice: The $x = 1/2$ CsCl (bcc-based) structure and the $x = 1/4$ and $3/4$ $D0_{22}$ (fcc-based) structures are ground states.

B. Competition between electrostatic and promotion energies

We wish to use the Madelung energies for structures based on the fcc, bcc, and sc lattices as a basis for the prediction of the relative stability of the CsCl, NaCl, and “40” structures in alloy systems. The Madelung energy

of a configuration σ based on the fcc, bcc, or sc lattices as depicted in Fig. 3 refers to an energy zero based on a concentration-weighted average of pure constituent energies *in the same lattice structure as σ* . In general, the lattice on which σ is based may not be the equilibrium structure of both the constituents of the alloy. Hence we must add the *promotion energy* which measures the energy required to transform a mixture of pure A and pure B with concentration x from one lattice structure to another. For example, the promotion energy from fcc to bcc may be written

$$E_{A+B}^{\text{fcc}} - E_{A+B}^{\text{bcc}} = (1-x)[E_A^{\text{fcc}} - E_A^{\text{bcc}}] + x[E_B^{\text{fcc}} - E_B^{\text{bcc}}]. \quad (17)$$

The elemental promotion energy, e.g., $E_A^{\text{fcc}} - E_A^{\text{bcc}}$, is a difference of total energies and has been calculated for most of the elements of the Periodic Table in a variety of lattice structures by several first-principles, total energy formulations.^{40–46} Note that $E_{A+B}^{\text{fcc}} - E_{A+B}^{\text{bcc}} > (<) 0$ if both the constituents of the alloy are stable in the bcc (fcc) structure. Equations similar to Eq. (17) may be written for fcc-sc and bcc-sc energy differences. We may then write the difference in total energy between a given configuration σ based on the fcc lattice and a configuration σ' based on the bcc lattice as the sum of the promotion energy $E_{A+B}^{\text{fcc}} - E_{A+B}^{\text{bcc}}$, the difference in Madelung energies, and a residual energy $E_{\text{res}}^{\text{fcc}}(\sigma) - E_{\text{res}}^{\text{bcc}}(\sigma')$, which accounts for all effects which are explicitly nonelectrostatic

$$\begin{aligned} \Delta E_{\sigma}^{\text{fcc}} - \Delta E_{\sigma'}^{\text{bcc}} = & [E_{A+B}^{\text{fcc}} - E_{A+B}^{\text{bcc}}] \\ & + [E_M^{\text{fcc}}(\sigma) - E_M^{\text{bcc}}(\sigma')] \\ & + [E_{\text{res}}^{\text{fcc}}(\sigma) - E_{\text{res}}^{\text{bcc}}(\sigma')]. \end{aligned} \quad (18)$$

We specifically wish to address the issue of structural stability in alloys which possess a high degree of ionicity, i.e., $E_M^{\text{fcc}}(\sigma) - E_M^{\text{bcc}}(\sigma')$ is dominant over $E_{\text{res}}^{\text{fcc}}(\sigma) - E_{\text{res}}^{\text{bcc}}(\sigma')$ in Eq. (18). We must then consider the relative magnitudes of the promotion energy and the Madelung energy. For alloys which have $E_{A+B}^{\text{fcc}} - E_{A+B}^{\text{bcc}} \simeq 0$ (and similarly for fcc-sc and bcc-sc promotion energies), the structural stability will be decided by the electrostatic

considerations (as shown in Fig. 3), which favor the stability of the CsCl structure. However, for most transition metals,⁴² the fcc-sc and bcc-sc promotion energies $E_{A+B}^{\text{fcc}} - E_{A+B}^{\text{sc}}$ and $E_{A+B}^{\text{bcc}} - E_{A+B}^{\text{sc}}$ are quite large and negative, indicating that the elemental metals in the sc structure have an energy that is quite high with respect to their equilibrium structure, which is most often fcc, bcc, or hcp. Paxton *et al.* show⁴² that for the 3d series Sc→Cu, the elemental fcc-sc and bcc-sc promotion energies are all negative and larger in magnitude than 0.5 eV/atom and may be as large as 1.0 eV/atom. Thus the energy of the sc-based alloy structures are very unstable with respect to the fcc- or bcc-based alloy structures. Consequently, even though the NaCl structure may accommodate a large negative electrostatic energy, this structure is never observed in transition metal alloys because any “gains” in Madelung energy are more than offset by large “costs” in the promotion energies.

We now consider the relative stability of fcc- and bcc-based alloy structures based on the interplay between electrostatic and promotion energy terms. We have schematically drawn the Madelung energies for the CsCl, “40,” and $D0_{22}$ structures for various values of the promotion energies in Fig. 4. If the fcc-bcc promotion energies are very small, the relative orders of fcc-bcc stability should be essentially those of Fig. 3, i.e., the CsCl structure is the most stable. However, if the promotion energies are large, the structural stability of the various compounds will be affected. In alloys with both constituents in the bcc structure [Figs. 4(a) and 4(b)], $E_{A+B}^{\text{fcc}} - E_{A+B}^{\text{bcc}} > 0$ and the stability of the CsCl structure due to electrostatic considerations is only *enhanced* by the promotion energies, regardless of their magnitude. However, the situation becomes more complicated in alloys for which one or more of the constituents is fcc. First, consider the case of an alloy in which one element is fcc and the other is bcc [Figs. 4(c) and 4(d)]. The competition between stability of the CsCl and “40” structures will then be decided by which constituent has the higher elemental promotion energy: If the bcc element has the higher promotion energy [as pictured in Fig. 4(c)], then $E_{A+B}^{\text{fcc}} - E_{A+B}^{\text{bcc}} > 0$ and the bcc-based CsCl will be lower in energy than “40”; however, if the fcc element has a higher promotion energy,

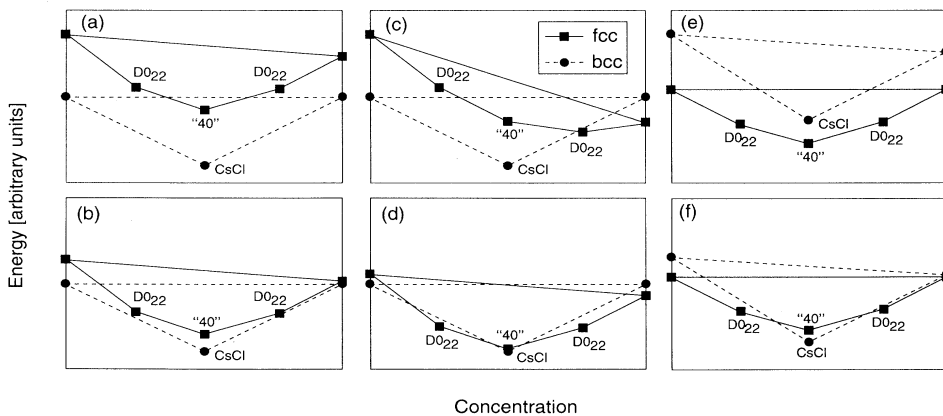


FIG. 4. Schematic representations of Madelung energies as a function of composition for ordered fcc- and bcc-based structures with various values of elemental promotion energies. The fcc- (bcc-) based structures are shown as squares (circles) connected by solid (dashed) lines.

$E_{A+B}^{\text{fcc}} - E_{A+B}^{\text{bcc}} < 0$ and the orders of stability could be reversed, provided that $E_{A+B}^{\text{fcc}} - E_{A+B}^{\text{bcc}}$ is sufficiently negative so as to overcome the difference between the CsCl and “40” electrostatic energies. If both elements of the alloy are fcc, the “40” structure will be stable if the promotion energies of one or both of the elements is large enough that $E_{A+B}^{\text{fcc}} - E_{A+B}^{\text{bcc}} \ll 0$ [Fig. 4(e)]. If both fcc elements have a small promotion energy [Fig. 4(f)], the CsCl structure will still be lower in energy due to electrostatic effects. Of the six possible scenarios depicted in Fig. 4, in only one case is “40” unambiguously predicted to be stable. Thus this provides a partial explanation for the near absence of experimentally observed²⁷ alloys with the “40” structure: For highly ionic systems, the “40” structure is the lowest energy *fcc-based structure*; however, the CsCl structure can accommodate an even more negative electrostatic energy. Thus in many ionic alloy systems, this bcc structure will form even if the constituents of the alloy are fcc, provided that the promotion energies of the elements are not too large (e.g., CuPd, AlNi, CaPd, etc.). However, *we predict that the “40” structure should be stable for an ionic alloy system composed of fcc elements, one or both of which possess a large fcc-bcc promotion energy.*

Many alloys (e.g., CuOs, AuIr, AgRu, LaRe, and CuRu) which possess the above criteria favoring formation of the “40” structure (high ionicity and a large fcc-bcc promotion energy) have formation energies which are positive,⁴⁷ implying phase separation rather than ordering. Thus, in these alloys, although we predict that the “40” structure should have an energy lower than the CsCl structure, a phase separated mixture of the constituents

($A + B$) will have an even lower energy and thus could be stable. Furthermore, our discussion has been limited mainly to the relative stabilities of the CsCl and “40” structures. In certain alloys, the residual, *nonelectrostatic* terms E_{res} can play a crucial role and even though the “40” structure may be stable with respect to the CsCl structure, another alloy configuration could prove to be still lower in energy. The above statements provide even more explanation for the relative scarcity of the observation of the “40” structure in binary alloys.

C. $T \neq 0$ K SRO in the bcc and sc Madelung lattices

The Monte Carlo and mean-field calculated SRO(\mathbf{k}) are contrasted in Fig. 5 for the unfrustrated bcc and sc Madelung lattices. The SRO in Fig. 5 is shown in the form of contour plots in the $(hk0)$ and (hkk) planes for the bcc and sc lattices, respectively. Black shading inside the highest contour locates the peaks in the SRO pattern. For the Monte Carlo calculations of the SRO, temperatures were chosen just above the order-disorder transition and the mean-field calculations were performed at a temperature such that the peak intensity of the mean-field SRO matched that of Monte Carlo. These temperatures are given in the caption of Fig. 5 and it may be seen that the mean-field temperatures are roughly 10–20% higher than the corresponding Monte Carlo values. This relatively small error in the mean-field approximation is not uncommon for situations in phase stability in which frustration plays only a minor role.¹⁵ The simulated annealing calculations indicate that the transitions

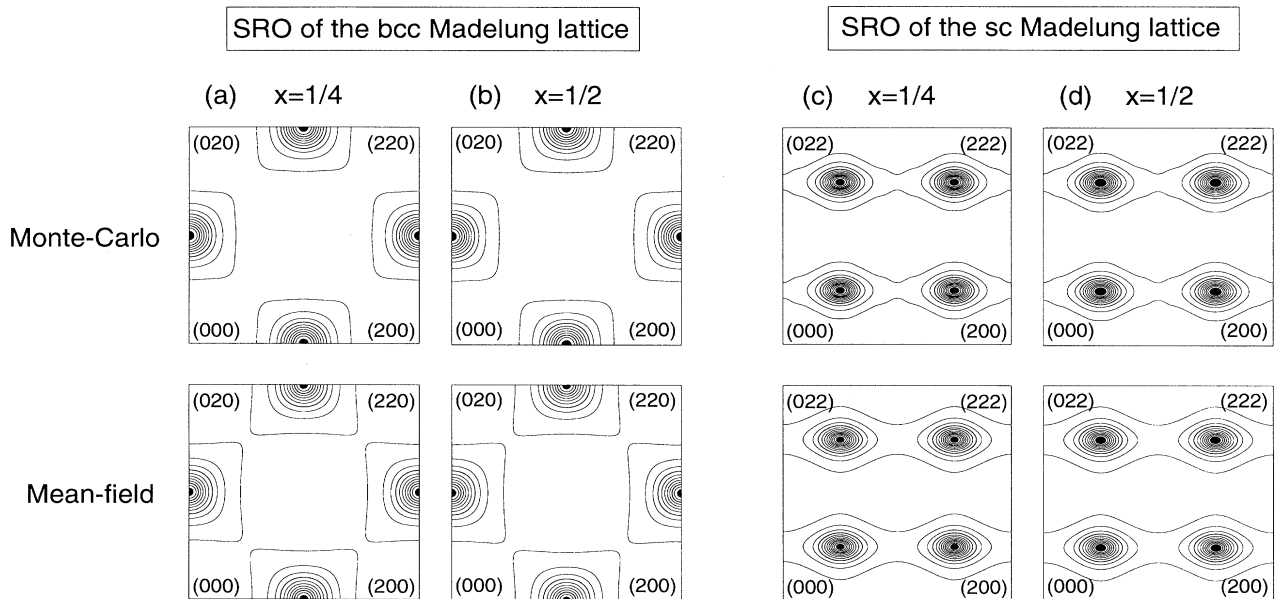


FIG. 5. Short-range order of the bcc [(a) and (b)] and sc [(c) and (d)] Madelung lattices for alloy compositions $x = 1/4$ and $1/2$. The Monte Carlo and mean-field calculated SRO patterns are shown as contour plots (in Laue units) in the $(hk0)$ plane for the bcc and the (hkk) plane for the sc Madelung lattice. The black shaded regions inside the highest contours locate the peaks in the SRO. The temperatures (in units of $Q_{\text{op}}^2/2dk_B$, where k_B is the Boltzmann constant) at which the Monte Carlo (mean-field) calculations were performed for (a)–(d) are 2.15 (2.53), 3.02 (3.37), 1.98 (2.41), and 2.84 (3.24).

from the high-temperature disordered phase to the low-temperature CsCl or NaCl structure are both second order (or weakly first order) and therefore without further refinements to the Monte Carlo (such as finite size scaling), we cannot give accurate values of the transition temperatures. The Monte Carlo calculations show that the SRO peaks at the $\langle 100 \rangle$ points for bcc and the $\frac{1}{2}\langle 111 \rangle$ points for sc lattices for all compositions. These \mathbf{k} vectors are identical to those for the long-range ordered CsCl and NaCl states, the $T=0$ K ground states for bcc and sc. Consequently, the mean-field calculations show remarkably good agreement with Monte Carlo.

**D. $T \neq 0$ K SRO in the fcc Madelung lattice:
A failure of mean-field theory**

The SRO(\mathbf{k}) for the fcc Madelung lattice from Monte Carlo and mean-field (with and without Onsager correc-

tions) calculations are contrasted in Fig. 6 as contour plots in the $(hk0)$ plane. Black shading inside the highest contour locates the peaks in the SRO patterns. The Monte Carlo calculations show the transitions on the fcc lattice to be first order (marked by a strong discontinuity in the internal energy as a function of temperature) and the transition temperatures are given in Table III. As in the bcc and sc cases, temperatures for the Monte Carlo calculation of the SRO were chosen just above the order-disorder transition (typically, $T_{\text{SRO}} = 1.02T_c$), and the mean-field calculations were performed at a temperature such that the peak intensity of the mean-field SRO matched that of the Monte Carlo calculation. These temperatures are given in the caption of Fig. 6. The mean-field calculations both with and without Onsager corrections in Fig. 6 show that at all compositions x , the SRO peaks at the $\langle 1\frac{1}{2}0 \rangle$ points, consistent with the nature of the LRO states, but in conflict with the Monte Carlo calculations (see also Table III). Thus the Onsager cor-

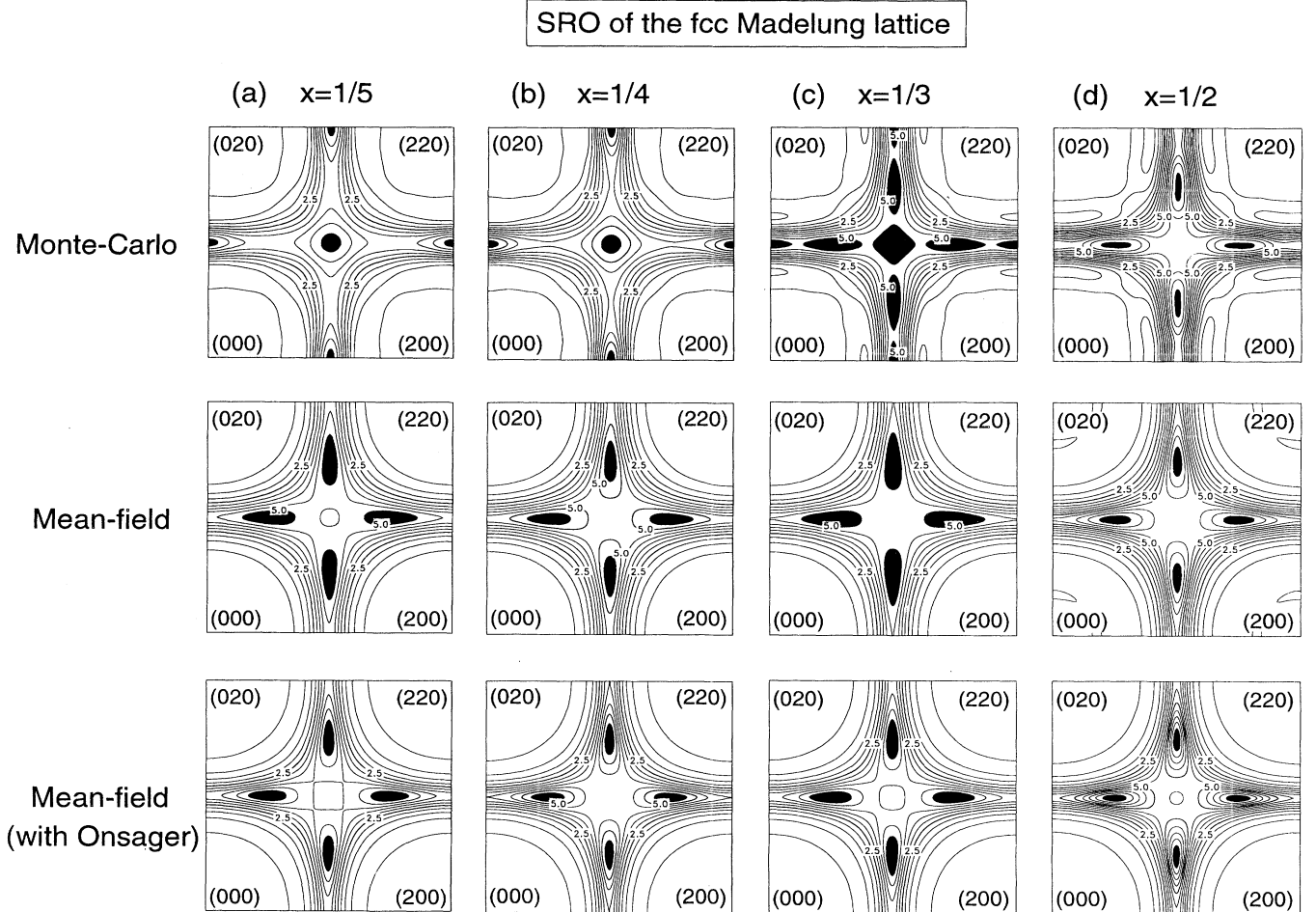


FIG. 6. Short-range order of the fcc Madelung lattice as a function of alloy composition x . The SRO patterns from Monte Carlo and mean-field (without and with Onsager corrections) calculations are shown for (a) $x = 1/5$, (b) $x = 1/4$, (c) $x = 1/3$, and (d) $x = 1/2$ as contour plots in the $(hk0)$ plane (in Laue units). The black shaded regions inside the highest contours locate the peaks in the SRO. The temperatures (in units of $Q_{\text{op}}^2/2dk_B$, where k_B is the Boltzmann constant) at which the Monte Carlo, the mean-field, and the mean-field with Onsager corrections calculations were performed are (a) 0.86, 1.41, 0.74; (b) 0.96, 1.62, 0.84; (c) 0.95, 1.95, 1.02; and (d) 0.93, 2.08, 1.00.

TABLE III. Properties of the fcc Madelung lattice as a function of composition x . The long-range ordered ground states are given, as are the reciprocal-space peak positions of the SRO, as determined by Monte Carlo (MC) and mean-field (MF) statistics. $\Delta E/\tilde{J}_1$ is the normalized $T=0$ Madelung energy difference between the $\langle 100 \rangle$ - and $\langle 1\frac{1}{2}0 \rangle$ -type structures normalized by the effective nearest-neighbor pair interaction \tilde{J}_1 . For $x = 1/4$ it is $\Delta E/\tilde{J}_1 = [E(L1_2) - E(D0_{22})]/\tilde{J}_1$ and for $x = 1/2$ it is $\Delta E/\tilde{J}_1 = [E(L1_0) - E(\text{"40"})]/\tilde{J}_1$. Transition temperatures T_c as determined by Monte Carlo are given in units of $(16\lambda)^2/2dk_B$, where k_B is the Boltzmann constant.

| Stoichiometry | $x = \frac{1}{5}$ A_4B | $x = \frac{1}{4}$ A_3B | $x = \frac{1}{3}$ A_2B | $x = \frac{1}{2}$ AB |
|------------------------|---------------------------------|---------------------------------|--|---------------------------------|
| Ground state | $A + D0_{22}$ | $D0_{22}$ | $D0_{22} + \text{"40"}$ | "40" |
| SRO (MC) | $\langle 100 \rangle$ | $\langle 100 \rangle$ | $\langle 100 \rangle, \langle 1\frac{1}{2}0 \rangle$ | $\langle 1\frac{1}{2}0 \rangle$ |
| SRO (MF) | $\langle 1\frac{1}{2}0 \rangle$ | $\langle 1\frac{1}{2}0 \rangle$ | $\langle 1\frac{1}{2}0 \rangle$ | $\langle 1\frac{1}{2}0 \rangle$ |
| $\Delta E/\tilde{J}_1$ | | +0.065 | | +0.130 |
| T_c (MC) | | 0.95 | | 0.91 |

rection does not change the dominant wave vectors of the SRO (this correction serves, however, to renormalize the temperature scale). In contrast to mean-field calculations, which show SRO peaks at the $\langle 1\frac{1}{2}0 \rangle$ points, the Monte Carlo calculations clearly show that the SRO peaks actually exist at the $\langle 100 \rangle$ points for $x = \frac{1}{5}$ and $\frac{1}{4}$, whereas for $x = \frac{1}{3}$, there are peaks at both the $\langle 1\frac{1}{2}0 \rangle$ and $\langle 100 \rangle$ points of nearly equal intensity. Of the compositions considered, only $x = \frac{1}{2}$ shows peaks at the $\langle 1\frac{1}{2}0 \rangle$ points, as computed by Monte Carlo. Thus, for several compositions, the dominant wave vectors of the SRO are not equivalent to those of the LRO, in qualitative contrast with mean-field theory.

The crossover between the $\langle 1\frac{1}{2}0 \rangle$ - and $\langle 100 \rangle$ -point SRO intensities is shown in Fig. 7. In this figure, the normalized SRO of type \mathbf{k} , i.e., $R(\mathbf{k}) = \text{SRO}(\mathbf{k})/[\text{SRO}(\mathbf{k}) + \text{SRO}(\mathbf{k}')]]$ is plotted (for $\mathbf{k}=\langle 1\frac{1}{2}0 \rangle$ and $\mathbf{k}'=\langle 100 \rangle$) as a function of alloy composition. The crossover occurs for compositions $x \sim 0.33$ and $x \sim 0.67$. The mean-field

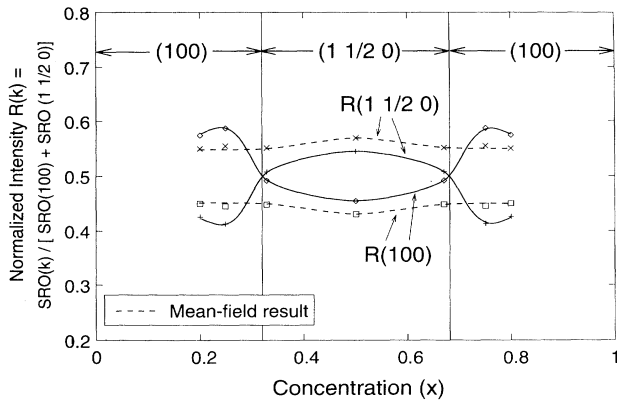


FIG. 7. $\langle 100 \rangle$ versus $\langle 1\frac{1}{2}0 \rangle$ SRO intensity for the fcc Madelung lattice as a function of alloy composition. The crossover between $\langle 100 \rangle$ - and $\langle 1\frac{1}{2}0 \rangle$ -point SRO occurs at $x \sim 0.33$ and $x \sim 0.67$ for the Monte Carlo calculations, whereas mean-field calculations of the SRO show no such crossover and indicate $\langle 1\frac{1}{2}0 \rangle$ -point SRO throughout the entire concentration range. (The symbols represent the actual calculated points; curves are drawn merely to guide the eye.) The Monte Carlo (mean-field) results are shown by the solid (dashed) curves.

calculations show no such crossover and thus fail qualitatively for $x \lesssim 0.33$ and $x \gtrsim 0.67$. Also, it should be noted that there exists no composition for which there is quantitative agreement between mean-field and Monte Carlo calculations.

The non-mean-field behavior of the SRO of the fcc Madelung lattice may be understood in terms of the model calculations of Fig. 8. In this figure, the normalized SRO of type \mathbf{k} at $x = \frac{1}{2}$ is plotted as a function of the energy difference $\Delta E = E(L1_0) - E(\text{"40"})$ normalized by \tilde{J}_1 . For $x = \frac{1}{4}$, we use $\Delta E = E(L1_2) - E(D0_{22})$. These calculations are performed for a variety of different sets and ranges of model effective interactions \tilde{J}_f (i.e., not those of the Madelung lattice). The solid vertical lines delineate $\langle 100 \rangle$ from $\langle 1\frac{1}{2}0 \rangle$ LRO and the dashed vertical lines separate $\langle 100 \rangle$ from $\langle 1\frac{1}{2}0 \rangle$ SRO, as computed by Monte Carlo. Thus the region between the vertical solid and dashed lines indicates regions of parameter space where the SRO is of $\langle 100 \rangle$ type while the LRO is of $\langle 1\frac{1}{2}0 \rangle$ type. Mean-field calculations exhibit no such region; thus we refer to this portion of parameter space as the "non-mean-field region." It was initially believed²⁹ that Pd_3V alloys should fall in this non-mean-field region since they are observed to exhibit $\langle 100 \rangle$ SRO and $\langle 1\frac{1}{2}0 \rangle$ LRO. However, it was later shown³⁰ that realistic interaction parameters place Pd_3V well outside this region, with $\mathbf{k}_{\text{SRO}} \neq \mathbf{k}_{\text{LRO}}$ in Pd_3V being due to finite-temperature excitations, which at high temperatures lower the value of $\Delta E/\tilde{J}_1$. As we see here, it is possible to have the non-mean-field behavior not only at $x = \frac{1}{4}$, but also at $x = \frac{1}{2}$, i.e., one can have $\langle 100 \rangle$ SRO coincident with a ground state of "40," composed entirely of $\langle 1\frac{1}{2}0 \rangle$ composition waves. Thus, since this non-mean-field behavior is possible at both $x = \frac{1}{4}$ and $x = \frac{1}{2}$, one might ask why it occurs for the Madelung model at $x = \frac{1}{4}$, but not at $x = \frac{1}{2}$. This question can be answered by considering the values of $\Delta E/\tilde{J}_1$ for the fcc Madelung lattice (given in Table III), in conjunction with the model calculations of Fig. 8 which involve interaction sets consisting of first-through fourth-nearest-neighbor pair interactions [Figs. 8(b) and 8(d)]. For $x = \frac{1}{4}$, the fcc Coulomb lattice has $\Delta E(L1_2 - D0_{22})/\tilde{J}_1 = +0.065$, which places it well within the non-mean-field region of Fig. 8(d), which extends from $0 < \Delta E(L1_2 - D0_{22})/\tilde{J}_1 \lesssim +0.14$. However, for

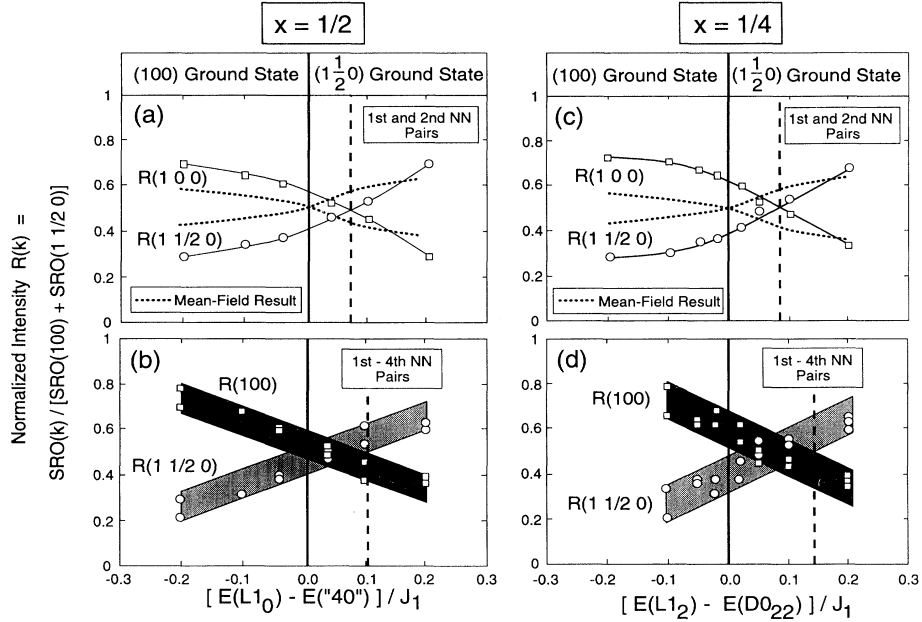


FIG. 8. Model calculations of the normalized SRO intensity $R(\mathbf{k})$ as a function of $\Delta E/\tilde{J}_1$ with (a) and (c) first- and second-neighbor pair interactions and (b) and (d) first- through fourth-neighbor pair interactions. Parts (a) and (b) indicate calculations performed for composition $x = 1/2$ and (c) and (d) indicate analogous calculations for $x = 1/4$. The squares and circles indicate the Monte Carlo results for $R(100)$ and $R(1\frac{1}{2}0)$, respectively. The Monte Carlo computations were all performed at $T = 1.1T_c$, and $T = 2.6T_c$ ($2.2T_c$) was used for the mean-field computations at $x = 1/2$ ($1/4$). In (b) and (d) the four pair model interactions were chosen at random with the constraints that no interaction (except \tilde{J}_1) has magnitude greater than $0.2\tilde{J}_1$ and all interactions sets for $x = 1/2$ ($1/4$) have as ground states either $L1_0$ or “40” ($L1_2$ or $D0_{22}$). The vertical solid (dashed) lines delineate $(1\frac{1}{2}0)$ from (100) LRO (SRO).

$x = \frac{1}{2}$, the fcc Coulomb lattice has $\Delta E(L1_0 - \text{“40”})/\tilde{J}_1 = +0.130$, precisely twice as large, and consequently does not fall within the non-mean-field region of Fig. 8(b), which encompasses $0 < \Delta E(L1_2 - D0_{22})/\tilde{J}_1 \lesssim +0.10$. Thus, due to the following two facts, the Madelung lattice does not exhibit non-mean-field behavior for $x = \frac{1}{2}$, but does for $x = \frac{1}{4}$: The non-mean-field region is slightly smaller and $\Delta E/\tilde{J}_1$ is twice as large for $x = \frac{1}{2}$ compared to $x = \frac{1}{4}$.

E. Implications of the failure of the mean-field theory of SRO

The qualitative failure of the mean-field theory of SRO [Eq. (14)] for the Madelung lattice has important ramifications for practitioners of electronic-structure techniques based on the single-site coherent-potential approximation (S-CPA). The energy of the random (R) alloy of composition x can be written as

$$E^{(R)}(x) = E_{\text{homog}}^{(R)}(x) + E_M^{(R)}(x) + E_{\text{relax}}^{(R)}(x). \quad (19)$$

Here the first term $E_{\text{homog}}^{(R)}(x)$ denotes the contribution of a hypothetical system lacking any correlations among the charges of site i and its neighbors $i+k$ [so $Q_i \propto \hat{S}_i$

and hence $E_M^{(R)} \equiv 0$] and any atomic relaxations (size effect). $E_{\text{homog}}^{(R)}(x)$ could therefore be obtained, in principle, for a huge supercell with $Q_i \propto \hat{S}_i$ using LDA. This term $E_{\text{homog}}^{(R)}(x)$ is often calculated^{25,26} by the S-CPA. The next two terms in Eq. (19) denote the contributions to the random alloy energy of correlated charge transfer and atomic relaxations, respectively. The calculations of the properties of the random alloy using the S-CPA neglect both correlations between charges [$E_M^{(R)}$ of Eq. (19)] and atomic relaxations [$E_{\text{relax}}^{(R)}$ of Eq. (19)]. Recently, a modification of the S-CPA has been adopted which accounts for the previously neglected nonzero Madelung contributions $E_M^{(R)}$ to the total energy of a random alloy which arise due to the correlations between charges.²¹ It was shown not only that this “charge-correlated” (CC) CPA produced formation energies of random alloys which were significantly disparate from those computed without charge correlations, but also that the inclusion of charge-correlations into the CPA lead to excess charges which depend very nearly linearly on the number of unlike nearest neighbors, i.e., that the CC-CPA was in quantitative agreement with Eq. (3) and hence in agreement with the Madelung model used in this paper. Thus the SRO calculations of the fcc Madelung lattice in this paper may be thought of (in terms of the CPA) as the *difference* in SRO one would calculate between using the S-CPA and the

CC-CPA. Many current SRO calculations based on the S-CPA (Refs. 26 and 32–35) employ the mean-field approximation but neglect charge correlations. Even if these SRO calculations are improved to include charge correlations, our results demonstrate that for fcc alloys with compositions $x \lesssim 0.33$ or $x \gtrsim 0.67$ a *mean-field statistical treatment (with or without Onsager corrections) will qualitatively fail* for the difference in SRO between the current calculations (with the S-CPA neglecting charge correlations) and ones that take into account Madelung contributions to the total energy.

F. The scale of Madelung energies in random and short-range ordered alloys

From Figs. 6 and 7 it is clear that the differences between fcc Monte Carlo and mean-field SRO computations are significant at the calculated temperatures, given in the caption of Fig. 6 in units of $(16\lambda)^2/2dk_B$. However, it still remains to assess the approximate scale of λ for real alloy systems and hence to determine whether or not the temperatures of the calculations in this paper correspond to a relevant range at which SRO is normally measured or computed. From Fig. 3 it is clear that the scale of the formation energies of the Madelung lattice (in units of $Q_{\text{op}}^2/2d$) is roughly equal to the scale of the temperatures used in this paper (in units of $Q_{\text{op}}^2/2dk_B$), as both these energies are of the order of one. Thus, if we could estimate the portion of the formation energy due to charge correlations of the random state for real alloy systems $\Delta E_M^{(R)}$, this would provide a rough estimate for the temperature scale of the calculations presented here T_M . Recent model calculations of $\Delta E_M^{(R)}$ come from several authors,^{21,48} who compared the formation energies of a few random $A_{1-x}B_x$ alloys using the S-CPA (which has a zero Madelung energy) and a charge transfer corrected CPA. The difference between these calculations gives us an estimate⁴⁹ of $\Delta E_M^{(R)}$:

$$\begin{aligned}\Delta E_M^{(R)}(\text{Cu}_{0.5}\text{Zn}_{0.5}) &= -1.25 \text{ mRy/atom}, T_M = 200 \text{ K}; \\ \Delta E_M^{(R)}(\text{Cu}_{0.5}\text{Au}_{0.5}) &= -5.3 \text{ mRy/atom}, T_M = 840 \text{ K};\end{aligned}\quad (20)$$

$$\begin{aligned}\Delta E_M^{(R)}(\text{Ni}_{0.5}\text{Al}_{0.5}) &= -7.7 \text{ mRy/atom}, T_M = 1200 \text{ K}; \\ \Delta E_M^{(R)}(\text{Li}_{0.5}\text{Al}_{0.5}) &= -16.0 \text{ mRy/atom}, T_M = 2500 \text{ K}.\end{aligned}$$

Additionally, Lu *et al.* give values²⁰ of $\lambda \approx 5.5 \times 10^{-3}$, 6.2×10^{-3} , and 1.3×10^{-2} for fcc $\text{Cu}_{0.5}\text{Pd}_{0.5}$, $\text{Cu}_{0.75}\text{Pd}_{0.25}$, and $\text{Cu}_{0.75}\text{Au}_{0.25}$ alloys, which lead to the estimates

$$\begin{aligned}\Delta E_M^{(R)}(\text{Cu}_{0.5}\text{Pd}_{0.5}) &= -1.1 \text{ mRy/atom}, T_M = 170 \text{ K}; \\ \Delta E_M^{(R)}(\text{Cu}_{0.75}\text{Pd}_{0.25}) &= -1.1 \text{ mRy/atom}, T_M = 170 \text{ K};\end{aligned}\quad (21)$$

$$\Delta E_M^{(R)}(\text{Cu}_{0.75}\text{Au}_{0.5}) = -4.8 \text{ mRy/atom}, T_M = 760 \text{ K}.$$

For the more ionic alloys, the addition of the Madelung energies results in significant changes in the calculated heats of formation, as the Madelung corrections are the

same order of magnitude as typical heats of mixing. In the Li-Al system, the magnitude of the Madelung energy of random alloys⁴⁸ is so large as to even change the *sign* of the calculated heats of formation. Also in the more ionic alloys, T_M is certainly consistent with the scale of temperatures at which SRO is normally measured. Thus, for ionic materials, the effects described in this paper are not small and could likely show a sizeable contribution to the diffuse scattered intensity.

It is interesting to compare the Madelung correction $\Delta E_M^{(R)}$ for the random alloy energy to the total mixing energy. The mixing energies of disordered alloys are experimentally measured not for the random state (which would only occur at infinite temperature), but rather for the short-range ordered state. Thus, in addition to the contributions of the random alloy given in Eq. (19), the mixing energy for disordered alloy at finite temperature has a contribution due to SRO:

$$\begin{aligned}\Delta E^{\text{mix}}(x, T) &= \Delta E_{\text{homog}}^{(R)}(x) + \Delta E_M^{(R)}(x) \\ &\quad + \Delta E_{\text{relax}}^{(R)}(x) + \delta E^{\text{SRO}}(x, T).\end{aligned}\quad (22)$$

Now δE^{SRO} , $\Delta E_M^{(R)}$, and $\Delta E_{\text{relax}}^{(R)}$ must all *lower* the mixing energy with respect to $\Delta E_{\text{homog}}^{(R)}$. Thus it is simply not appropriate to compare $\Delta E_{\text{homog}}^{(R)}$ (as, e.g., computed by the S-CPA) with values of ΔE^{mix} given by experiment, unless one has independently verified that the contributions δE^{SRO} , $\Delta E_M^{(R)}$, and $\Delta E_{\text{relax}}^{(R)}$ are all small. For $\text{Cu}_{0.5}\text{Au}_{0.5}$ alloys, there are estimates of all the terms of Eq. (22) reported in the literature: Weinberger *et al.*⁵⁰ have recently reported $\Delta E_{\text{homog}}^{(R)} = -57$ meV/atom for $\text{Cu}_{0.5}\text{Au}_{0.5}$, using a fully relativistic S-CPA. Johnson and Pinski²¹ calculated $\Delta E_M^{(R)} = -72$ meV/atom and Amador and Bozzolo⁵¹ calculated $\delta E^{\text{SRO}} = -65$ meV/atom. As for $\Delta E_{\text{relax}}^{(R)}$, Lu *et al.*²⁴ calculated the relaxation for the *ordered* CuAu structure to be -29 meV/atom. The value is presumably more negative for the random alloy having lower symmetry. Thus it is clear that for $\text{Cu}_{0.5}\text{Au}_{0.5}$, a comparison⁵⁰ of $\Delta E_{\text{homog}}^{(R)}$ directly with the experimental values of -53 or -71 meV/atom (Ref. 52) neglects contributions δE^{SRO} , $\Delta E_M^{(R)}$, and $\Delta E_{\text{relax}}^{(R)}$, which may contribute as much as -170 meV/atom to the mixing energy.

The term $\delta E^{\text{SRO}}(x, T)$ in Eq. (22) due to SRO implicitly contains contributions due to the homogeneous medium, Madelung corrections, and relaxations. Thus the mixing energy of the short-range ordered Madelung lattice may be divided into a contribution of the random alloy and a correction due to SRO:

$$\Delta E_M^{\text{mix}}(x, T) = \Delta E_M^{(R)}(x) + \delta E_M^{\text{SRO}}(x, T).\quad (23)$$

It is interesting to determine the size of each of the contributions $\Delta E_M^{(R)}$ and δE_M^{SRO} . Figure 9 shows the internal energy versus temperature for the fcc Madelung lattice at $x = 0.5$, as calculated by Monte Carlo simulated annealing. Even up to a temperature that is four times the transition temperature, the effect of SRO on the energy

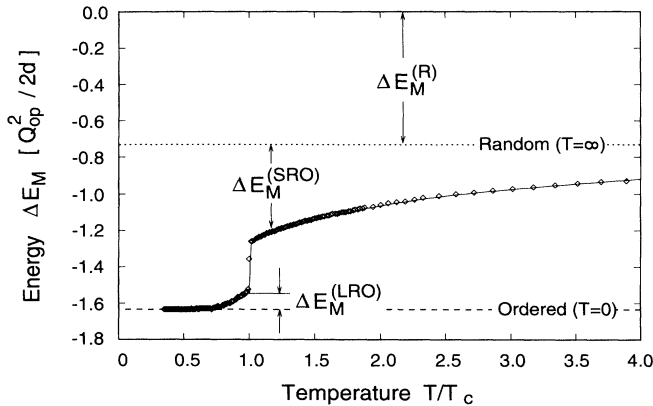


FIG. 9. Internal energy as a function of temperature for the fcc Madelung lattice at $x = 1/2$. Indicated are the contributions to the Madelung energy due to (i) the random alloy, (ii) the short-range ordered alloy (the difference between the calculated energy at finite $T > T_c$ and the energy at infinite temperature), and (iii) the long-range ordered alloy (the difference between the calculated energy at finite $T < T_c$ and the energy at $T = 0$ K). Note the sharp discontinuity at $T = T_c$ as the alloy undergoes a first-order transition between the disordered and LRO (“40”) state.

is sizeable, as the δE_M^{SRO} at $T = 4T_c$ is roughly 25% of $\Delta E_M^{(R)}$. At temperatures closer to T_c , the effect due to SRO is amplified and the energy of the SRO state may be $\gtrsim 60\%$ lower than the random alloy energy. Also shown in Fig. 9 is the contribution to ΔE_M due to LRO, i.e., the difference between ΔE_M of the completely ordered state and that at finite $T < T_c$. In contrast to the effect of SRO, $\Delta E_M(\text{LRO})$ appears to be quite small, even at temperatures close to T_c . Thus, any attempts to compare theoretical formation energies of disordered alloys with those of experiment should of course include the contributions to SRO. As has been recently demonstrated⁵¹ for *total* energies, the contributions due to SRO can be quite sizeable: For the slightly reactive alloys $\text{Ni}_{0.5}\text{Pt}_{0.5}$ and $\text{Cu}_{0.5}\text{Au}_{0.5}$, Amador and Bozzolo⁵¹ have estimated the effects of SRO on the energy of mixing to be roughly -70 meV/atom at temperatures slightly above the experimental order-disorder transition. In both of these materials, the inclusion of SRO is shown to reverse the *sign* of energy of mixing, compared with a calculation of the completely random alloy. We show here that, for ionic materials, any attempt to include Madelung contributions to the formation energy of a disordered alloy must include not only the random state Madelung energy, but also the contributions due to SRO.

V. CONCLUSIONS

We have examined the long- and short-range order of the binary Madelung fcc, bcc, and sc lattices. Our results are based on the charge model of Eq. (3), which has been shown^{20–22} to be correct for transition metal and semiconductor alloys by first-principles charge density calcu-

TABLE IV. Dominant wave vectors of the long- and short-range order for the fcc, bcc, and sc Madelung lattices.

| Lattice | LRO | | SRO | |
|---------|------------------|----------------------------------|----------------------------------|----------------------------------|
| | Ground states | Wave vector | Wave vectors | |
| | | | $x = \frac{1}{4}$ | $x = \frac{1}{2}$ |
| fcc | $D0_{22}$, “40” | $\langle 1\frac{1}{2}0 \rangle$ | $\langle 100 \rangle$ | $\langle 1\frac{1}{2}0 \rangle$ |
| bcc | CsCl ($B2$) | $\langle 100 \rangle$ | $\langle 100 \rangle$ | $\langle 100 \rangle$ |
| sc | NaCl ($B1$) | $\frac{1}{2}\langle 111 \rangle$ | $\frac{1}{2}\langle 111 \rangle$ | $\frac{1}{2}\langle 111 \rangle$ |

lations. The ground states and dominant wave vectors for long- and short-range order are summarized in Table IV. We find the following. (i) We confirm the results of Magri *et al.*¹⁹ that the three lowest energy configurations of the fcc Madelung lattice are the $D0_{22}$ (A_3B and AB_3) and “40” (AB) structures, all of which are composed out of composition waves along the $\langle 1\frac{1}{2}0 \rangle$ direction. Additionally, we find the ground states of the bcc and sc Madelung lattices to be the CsCl and NaCl structures, composed entirely out of $\langle 100 \rangle$ and $\frac{1}{2}\langle 111 \rangle$ composition waves, respectively. (ii) The bcc-based CsCl structure has the highest Madelung constant of any fcc-, bcc-, or sc-based structure. (iii) For the unfrustrated bcc and sc lattices, the wave vectors of SRO coincide with those of LRO, as would be predicted by a mean-field theory. Consequently, Monte Carlo and mean-field calculations of the SRO agree well for these cases. (iv) For the frustrated fcc lattice at $x = 1/2$, both Monte Carlo and mean-field calculations show the dominant wave vectors of the SRO to be $\langle 1\frac{1}{2}0 \rangle$. (v) However, for $x \lesssim 0.33$ and $x \gtrsim 0.67$, Monte Carlo results show SRO which peaks at the $\langle 100 \rangle$ points, in qualitative contrast to mean-field theory, which predicts peaks at the $\langle 1\frac{1}{2}0 \rangle$ points. Thus, for the diffuse scattering contribution due to electrostatics in fcc alloys, mean-field theory qualitatively fails, as the dominant wave vectors of LRO do not coincide with those of SRO. (vi) This non-mean-field behavior of the SRO has a serious implication with respect to calculations based on the coherent-potential approximation: Mean-field calculations of the *difference* in SRO between the standard- and charge-transfer-corrected CPA will fail qualitatively. (vii) The energy and temperature scales of the Madelung model presented here have been assessed and it is found that the contributions of Madelung energy to structural stability and diffuse scattered intensity due to SRO may be quite large for ionic alloys. (viii) The contribution of SRO to the energetics of the Madelung model near the transition temperature is $\gtrsim 60\%$ of that due to the completely random alloy. Thus any attempt to compare calculated and experimental formation energies of disordered alloys must include not only the Madelung energy of the random alloy, but also the electrostatic contribution due to SRO.

ACKNOWLEDGMENT

This work was supported by the Office of Energy Research (Division of Materials Science of the Office of Basic Energy Sciences), U.S. Department of Energy, under Contract No. DE-AC36-83CH10093.

- ¹ M. P. Tosi, in *Solid State Physics*, edited by F. Seitz and D. Turnbull, (Academic, New York, 1964), Vol. 16.
- ² L. C. Pauling, *The Nature of the Chemical Bond and the Structure of Molecules and Crystals: An Introduction to Modern Structural Chemistry* (Cornell University Press, Ithaca, NY, 1960).
- ³ W. B. Pearson, *The Crystal Chemistry and Physics of Metals and Alloys* (Wiley-Interscience, New York, 1972).
- ⁴ M. van Schilfgaarde, A.-B. Chen, and A. Sher, *Phys. Rev. Lett.* **57**, 1149 (1986); S.-H. Wei, *ibid.* **59**, 2613 (1987).
- ⁵ W. Hume-Rothery, R. E. Smallman, and C. W. Haworth, *Structure of Metals and Alloys*, 5th ed. (Institute of Metals, London, 1969).
- ⁶ L. S. Darken and R. W. Gurry, *Physical Chemistry of Metals* (McGraw-Hill, New York, 1953).
- ⁷ A. R. Miedema, F. R. de Boer, and P. F. de Chatel, *J. Phys. F* **3**, 1558 (1973); A. R. Miedema, F. R. de Boer, and R. Boom, *CALPHAD* **1**, 341 (1977); A. R. Miedema, *J. Less-Common Met.* **32**, 117 (1973).
- ⁸ K. Levin and H. Ehrenreich, *Phys. Rev. B* **3**, 4172 (1971); R. E. Watson, J. Hudis, and M. L. Perlman, *ibid.* **4**, 4139 (1971).
- ⁹ J. Ihm, A. Zunger, and M. L. Cohen, *J. Phys. C* **12**, 4409 (1979).
- ¹⁰ S.-H. Wei and H. Krakauer, *Phys. Rev. Lett.* **55**, 1200 (1985), and references cited therein.
- ¹¹ M. Born, *Atomtheorie des festen Zustandes* (Teubner, Leipzig, 1923).
- ¹² P. P. Ewald, *Ann. Phys. (N.Y.)* **64**, 253 (1921).
- ¹³ J. Kanamori and Y. Kakehashi, *J. Phys. (Paris) Colloq.* **38**, C7-274 (1977).
- ¹⁴ J. M. Sanchez, F. Ducastelle, and D. Gratias, *Physica A* **128**, 334 (1984).
- ¹⁵ D. de Fontaine, *Solid State Phys.* **34**, 73 (1979).
- ¹⁶ F. Ducastelle, *Order and Phase Stability in Alloys* (Elsevier, New York, 1991).
- ¹⁷ For a collection of articles, see *Alloy Phase Stability*, Vol. 163 of *NATO Advanced Study Institute, Series B: Physics*, edited by G. M. Stocks and A. Gonis, (Kluwer, Dordrecht, 1989); *Statics and Dynamics of Alloy Phase Transformations*, Vol. 319 of *NATO Advanced Study Institute, Series B: Physics*, edited by P. E. A. Turchi and A. Gonis (Plenum, New York, 1994).
- ¹⁸ A. Zunger, in *Statics and Dynamics of Alloy Phase Transformations*, (Ref. 17), p. 361.
- ¹⁹ R. Magri, S.-H. Wei, and A. Zunger, *Phys. Rev. B* **42**, 11 388 (1990).
- ²⁰ Z. W. Lu, S.-H. Wei, and A. Zunger, *Phys. Rev. B* **44**, 10 470 (1991); **45**, 10 314 (1992).
- ²¹ D. D. Johnson and F. J. Pinski, *Phys. Rev. B* **48**, 11 553 (1993).
- ²² S.-H. Wei (unpublished) has performed first-principles LAPW calculations for the charge density of many equal-volume configurations of the zinc-blende semiconductor alloy $\text{Ga}_{1-x}\text{In}_x\text{P}$ and finds that the charge model of Eq. (3) accurately describes the excess charges on the P sites.
- ²³ First-principles charge density calculations have shown Eq. (3) to be reliable for screened solids such as transition metal and semiconductor alloys. However, to the authors' knowledge, there have been no similar studies for ionic solids. It would therefore be of interest to determine whether such halide and oxide systems are sufficiently screened so as to be described by Eq. (3).
- ²⁴ Z. W. Lu, S.-H. Wei, A. Zunger, S. Frota-Pessoa, and L. G. Ferreira, *Phys. Rev. B* **44**, 512 (1991).
- ²⁵ D. D. Johnson, D. M. Nicholson, F. J. Pinski, B. L. Gyorffy, and G. M. Stocks, *Phys. Rev. B* **41**, 9701 (1990).
- ²⁶ For a review of the coherent potential approximation, see B. L. Gyorffy, D. D. Johnson, F. J. Pinski, D. M. Nicholson, and G. M. Stocks, in *Alloy Phase Stability* (Ref. 17), p. 293; F. Ducastelle, *Order and Phase Stability in Alloys* (North-Holland, New York, 1991).
- ²⁷ Out of more than 50 000 intermetallic phases reported, Villars and Calvert [P. Villars and L. D. Calvert, *Pearson's Handbook of Crystallographic Data for Intermetallic Phases* (ASM International, Materials Park, OH, 1991)] list only NbP and PTa as intermetallics with the "40" structure (space group $I4_1/amd$). They also give a few references to a distorted version (space group $I4_1md$) of the "40" structure (e.g., AsNb, and AsTa).
- ²⁸ M. A. Krivoglaz and A. A. Smirnov, *The Theory of Order-Disorder in Alloys* (McDonald, London, 1964); P. C. Clapp and S. C. Moss, *Phys. Rev.* **142**, 418 (1966).
- ²⁹ F. Solal, R. Caudron, F. Ducastelle, A. Finel, and A. Loiseau, *Phys. Rev. Lett.* **58**, 2245 (1987).
- ³⁰ C. Wolverton, A. Zunger, and Z.-W. Lu, *Phys. Rev. B* **49**, 16 058 (1994).
- ³¹ Z.-W. Lu and A. Zunger, *Phys. Rev. B* **50**, 6626 (1994).
- ³² J. B. Staunton, D. D. Johnson, and F. J. Pinski *Phys. Rev. B* **50**, 1450 (1994); D. D. Johnson, J. B. Staunton, and F. J. Pinski, *ibid.* **50**, 1473 (1994).
- ³³ F. J. Pinski, B. Ginatempo, D. D. Johnson, J. B. Staunton, G. M. Stocks, and B. L. Gyorffy, *Phys. Rev. Lett.* **66**, 766 (1991).
- ³⁴ J. B. Staunton, D. D. Johnson, and F. J. Pinski, *Phys. Rev. Lett.* **65**, 1259 (1990).
- ³⁵ D. D. Johnson, J. B. Staunton, F. J. Pinski, B. L. Gyorffy, and G. M. Stocks, in *Applications of Multiple Scattering Theory to Materials Science*, edited by W. H. Butler, P. H. Dederichs, A. Gonis, and R. L. Weaver, *MRS Symposia Proceedings No. 253* (Materials Research Society, Pittsburgh, 1992).
- ³⁶ For more details of the simulated annealing calculations, the reader is referred to Z.-W. Lu, D. B. Laks, S.-H. Wei, and A. Zunger, *Phys. Rev. B* **50**, 6642 (1994).
- ³⁷ C. Wolverton, G. Ceder, D. de Fontaine, and H. Dreyssè, *Phys. Rev. B* **48**, 726 (1993); C. Wolverton, Ph. D. dissertation, University of California, Berkeley, 1993.
- ³⁸ Mean-field calculations of the SRO were compared using the first five (\bar{J}_{1-5}) and the first twenty pair interactions (\bar{J}_{1-20}) for the fcc Madelung lattice. The peak positions were unchanged by using longer-ranged interactions and the amplitude of the SRO at the peak position was affected by $\lesssim 1\%$. Thus we neglect the collective effects of the effective interactions beyond the fifth neighbor distance.
- ³⁹ P. R. Subramanian and D. E. Laughlin, *J. Phase Equilibria* **12**, 231 (1991).
- ⁴⁰ H. Skriver, *Phys. Rev. B* **31**, 1909 (1985).
- ⁴¹ J. W. Davenport, R. E. Watson, and M. Weinert, *Phys. Rev. B* **32**, 4883 (1985).
- ⁴² A. T. Paxton, M. Methfessel, and H. M. Polatoglou, *Phys. Rev. B* **41**, 8127 (1990).
- ⁴³ G. W. Fernando, R. E. Watson, M. Weinert, Y. J. Wang, and J. W. Davenport, *Phys. Rev. B* **41**, 11 813 (1990).
- ⁴⁴ J. M. Wills, O. Eriksson, P. Soderlind, and A. M. Boring, *Phys. Rev. Lett.* **68**, 2802 (1992).
- ⁴⁵ M. Sigalas, D. A. Papaconstantopoulos, and N. C. Bacalis, *Phys. Rev. B* **45**, 5777 (1992).

- ⁴⁶ V. Ozolins and M. Korling, Phys. Rev. B **48**, 18 304 (1993).
- ⁴⁷ F. R. de Boer, R. Boom, W. C. M. Mattens, A. R. Miedema, and A. K. Niessen, *Cohesion in Metals: Transition Metal Alloys* (North Holland, New York 1989).
- ⁴⁸ P. A. Korzhavyi, A. V. Ruban, S. I. Simak, and Yu. Kh. Vekilov, Phys. Rev. B **49**, 14 229 (1994).
- ⁴⁹ In characterizing the charge density in terms of charge transfer, one is faced with the fact that there is no unique way to apportion a three-dimensional solid into simple sub-units. All of the values of $\Delta E_M^{(R)}$ given in Sec. IV F should therefore be seen merely as rough estimates due to the nonunique characterization of charge transfer. Of course, the electrostatic energy is a well-defined quantity in first-principles calculations and one can always define a charge transfer parameter in a *model* calculation such that the model electrostatic energy equals that obtained in first-principles calculations.
- ⁵⁰ P. Weinberger, V. Drchal, L. Szunyogh, J. Fritscher, and B. I. Bennett, Phys. Rev. B **49**, 13 366 (1994).
- ⁵¹ C. Amador and G. Bozzolo, Phys. Rev. B **49**, 956 (1994).
- ⁵² R. L. Orr, Acta Metall. **8**, 489 (1960).